The hydrodynamic function of shark skin and two biomimetic applications

The Journal of Experimental Biology 215, 785-795

doi:10.1242/jeb.063040

RESEARCH ARTICLE

The hydrodynamic function of shark skin and two biomimetic applications

Johannes Oeffner and George V. Lauder*

Museum of Comparative Zoology, Harvard University, 26 Oxford Street, Cambridge, MA 02138, USA

*Author for correspondence (glauder@oeb.harvard.edu)

Accepted 16 November 2011

SUMMARY

It has long been suspected that the denticles on shark skin reduce hydrodynamic drag during locomotion, and a number of man-made materials have been produced that purport to use shark-skin-like surface roughness to reduce drag during swimming. But no studies to date have tested these claims of drag reduction under dynamic and controlled conditions in which the swimming speed and hydrodynamics of shark skin and skin-like materials can be quantitatively compared with those of controls lacking surface ornamentation or with surfaces in different orientations. We use a flapping foil robotic device that allows accurate determination of the self-propelled swimming (SPS) speed of both rigid and flexible membrane-like foils made of shark skin and two biomimetic models of shark skin to measure locomotor performance. We studied the SPS speed of real shark skin, a silicone riblet material with evenly spaced ridges and a Speedo® 'shark skin-like' swimsuit fabric attached to rigid flat-plate foils and when made into flexible membrane-like foils. We found no consistent increase in swimming speed with Speedo® fabric, a 7.2% increase with riblet material, whereas shark skin membranes (but not rigid shark skin plates) showed a mean 12.3% increase in swimming speed compared with the same skin foils after removing the denticles. Deformation of the shark skin membrane is thus crucial to the drag-reducing effect of surface denticles. Digital particle image velocimetry (DPIV) of the flow field surrounding moving shark skin foils shows that skin denticles promote enhanced leading-edge suction, which might have contributed to the observed increase in swimming speed. Shark skin denticles might thus enhance thrust, as well as reduce drag.

Key words: shark skin, locomotion, riblet, drag reduction, foil, swimming, Fastskin®.

INTRODUCTION

In recent decades, the skin of sharks has achieved a certain biomimetic status among both science popularizers and in research circles for the notion that the specialized skin surface structure could reduce drag and enhance the efficiency of locomotion. Manufactured body suits have been loosely modeled on shark skin with various ridges and dents, to induce surface roughness, that purportedly enhance swimming performance in humans, and researchers have long suspected that the special surface structure of shark skin contributes to the efficiency of locomotion [shark skin structure has been comprehensively reviewed (e.g. Applegate, 1967; Lang et al., 2008; Reif, 1982; Reif, 1985); also see images in Castro (Castro, 2011)].

A variety of 'shark-inspired' engineered materials have also been produced to reduce drag when applied to the surface of submerged bodies. For example, riblets are fine rib-like surface geometries with sharp surface ridges that can be aligned either parallel or perpendicular to the flow direction and might reduce drag. A diversity of riblet shapes and sizes has been investigated experimentally and theoretically (Bechert and Bartenwerfer, 1989; Bechert et al., 2000; Bechert et al., 1997; Büttner and Schulz, 2011; Koeltzsch et al., 2002; Luchini et al., 1991; Luchini and Trombetta, 1995; Neumann and Dinkelacker, 1991), and drag reduction of stiff bodies covered with riblet material has been shown to occur (Bechert et al., 1997; Bechert et al., 1985; Dinkelacker et al., 1987). Experiments with an adjustable surface with longitudinal blade ribs and slits revealed the highest stiff-body drag reduction of 9.9%, with a groove depth of half the size of lateral riblet spacing (Bechert et al., 1997). Scalloped riblets, somewhat similar to the ridges in shark denticles, produce a maximal stiff-body drag reduction of approximately 7% (Bechert et al., 1985).

A silicone-replica of the skin of the copper shark *Carcharhinus brachyurus* attached to a rigid flat plate resulted in a drag reduction of 5.2–8.3% compared with that of smooth silicone on a flat plate (Han et al., 2008). A hard plastic shark skin replica achieved a drag reduction of 3% (Bechert et al., 1985). But these cases involved study of a rigid body covered with a biomimetic skin, which is not the situation for a shark *in vivo*, where body undulations can greatly alter the structure of surface ornamentation and change flow characteristics over the skin. In addition, a variety of tests with the Speedo® FS II swimsuit 'shark-like' material resulted in a 7.7% (Benjanuvatra et al., 2002) and 10–15% (Mollendorf et al., 2004) reduction in the stiff-body drag compared with that of normal swimsuits under certain conditions, but other studies or tests showed no significant drag reduction (Benjanuvatra et al., 2002; Toussaint et al., 2002).

Because sharks are self-propelled deforming bodies, thrust and drag forces are hard to decouple (Anderson et al., 2001; Schultz and Webb, 2002; Tytell, 2007; Tytell et al., 2010), which makes it difficult to isolate drag forces alone during normal free-swimming locomotion to assess the effect of surface ornamentation. In order to investigate the possible drag-reducing properties of surface ornamentation such as shark skin denticles or various biomimetic products (or whether surface structures might possibly enhance thrust), it is necessary to use a study system that permits (1) the use of self-propelling bodies possessing different surface ornamentations, where thrust and drag forces are naturally balanced throughout an undulatory cycle, (2) accurate measurement of self-

propelled swimming (SPS) speed so that the swimming performance of different surfaces can be compared statistically, (3) the imposition of different motion programs so that the effect of moving the ornamented surfaces in different manners can be assessed, and (4) various experimental manipulations of surface structure to test directly the hypothesis that it is the surface ornamentation alone that causes drag reduction and hence increased swimming speed.

In this study, we use a robotic flapping foil device to test the effect of shark skin surface ornamentation and two biomimetic surfaces on SPS speed. The flapping foil robotic device was developed for the study of fish-like self-propulsion in both rigid and flexible foils and allows accurate measurement of free-swimming speeds, the production of controlled motion programs to move foils under a variety of heave and pitch conditions (Lauder et al., 2007; Lauder et al., 2011a; Lauder et al., 2011b) and quantification of flow over the foil surface using digital particle image velocimetry (DPIV). We make foils that are both rigid and flexible out of fresh shark skin and also study the propulsion of two manufactured shark skin mimics. We directly test the hypothesis in each case that surface ornamentation produces an increase in swimming speed by comparing against a control condition with reduced or absent ornamentation.

MATERIALS AND METHODS

Flapping foil materials

We produced foils to be mounted in the robotic flapping device with three different surface materials: Speedo® Fastskin FS II fabric, riblet material and real shark skin. Flexible moving foils with Speedo® Fastskin FS II fabric (provided by Speedo® International, Nottingham, UK) were produced. Two rectangular fabric pieces (20×7 cm) were bonded together using adhesive spray glue (Duro Spray Adhesive, Henkel, OH, USA) and clamped in a metal sandwich bar holder (consisting of two rectangular metal rods of 0.15×1×28 cm, identical to the one shown in Fig. 3) vertically and horizontally, respectively. Every foil is manufactured three times. In two foils, the outside (biomimetic surface, see Fig. 6B) of the Speedo® fabric faced the fluid, with the dent structure parallel and perpendicular to the flow, respectively. In the third foil, the smoother underside (not biomimetic surface, see Fig. 6A) of the fabric faced the fluid.

A rubber riblet membrane (average thickness of 1 mm) was made of silicone (Elastosil M 4630, Wacker Silicone, Drawin Vertriebs, Germany) by pouring the silicone on a lenticular foil, resulting in longitudinal U-shaped riblet structures with a height of 87 μm and a spacing of 340 μm (see Fig. 7). The rubber riblet material was glued (using adhesive spray glue, Duro Spray Adhesive, Henkel, OH, USA) onto a 19 cm long metal NACA 0012 foil with a chord length of 6.85 cm. Every foil was manufactured three times. In two foils, the outside (biomimetic surface, see Fig. 7A) of the riblet material faced the fluid, with the dent structure parallel (standard orientation of riblets) and perpendicular to the flow, respectively. In the third foil, the smooth underside (not biomimetic surface) of the fabric faced the fluid.

Both rigid and flexible shark skin foils were made with the skin of a male shortfin mako (*Isurus oxyrinchus* Rafinesque) with a total body length (BL) of 190 cm and a male porbeagle [*Lamna nasus* (Bonnaterre)] with a BL of 155 cm. Both species are fast-swimming sharks [according to the classifications of Reif (Reif, 1985)]. Both individuals were obtained shortly after being caught by fisherman off Boston, Massachusetts, USA, and had not been frozen at the time we first removed the skin. Skin panels were extracted using dissection instruments and cleaned with a water jet to remove any surface material that had adhered as a result of capture and transport. Scraping the underside of the skin with a single-edge razor blade mechanically removed attached muscle fibres and generated a skin membrane that could be attached to either a rigid foil or another piece of skin to make a bilaminar flexible skin membrane with the surface ornamentation facing out.

Rigid shark skin foils were made with skin pieces (6.5×17.5 cm, with an average thickness of 3 mm), at the longitudinal position of the dorsal fin, removed along the lateral side of the shortfin mako and were glued to both sides of a flat plate (3.1×6.8×19 cm) using a thin layer of commercially available cyanoacrylate 'Instant Krazy Glue' (Elmers Products, OH, USA). The denticle ridges were orientated parallel to the chord length of the foil. Semicircular hollow metal bars with a diameter of 8.17 cm (length 17.5 cm) were glued to the long edges of the foil to obtain smooth leading and trailing edges. The 'mako flat plate' foil (Fig. 2) has an uncovered top (breadth 1.5 cm) where the foil holder is attached. The symmetry of the flat-plate foil allows experiments to be conducted in two orientations by simply reversing the foil orientation in the robotic flapper: in-flow, where the denticle crown tips point downstream (as in the live shark), and against-flow, with upstream-facing crown tips.

Three flexible 'shark skin membrane' foils were produced: two with skin of the shortfin mako (no. 1 and no. 2) and one with skin of the porbeagle. For every foil, rectangular skin pieces with a size of 6.4×9.2 cm were extracted from below the dorsal fin (10 cm above the midline) of both lateral sides and bonded together. Skin membranes were clamped in two rectangular metal rods (0.15×1×28 cm) so that the denticle ridges were oriented parallel to the chord length and with the denticle crown peaks facing downstream (Fig. 3) – equivalent to the alignment in living sharks. The leading edge was sealed with epoxy to form an even, sharp leading edge and to prevent delamination of the glued membrane.

After finishing the self-propelled measurements with the intact foils, the denticles on each shark skin foil were removed by carefully sanding the skin surface under a microscope with wetted sandpaper (aluminum-oxide cloth) in order to design a control object (sanded foil) with the properties of shark skin but greatly reduced surface ornamentation (discussed further below). We tried a number of methods of removing denticles, but none was as effective as careful sanding under a microscope. We avoided chemical removal methods in order not to affect skin flexural stiffness. Although this method did not remove every denticle, and small nubs of the denticle bases were left on the surface, we found that more-aggressive denticle removal methods damaged the skin surface. Sanding did not remove the epidermis of the underlying skin.

Surface imaging

In this study, an environmental scanning electron microscope [(ESEM) Zeiss EVO SEM 50, Carl Zeiss SMT, NJ, USA] was used in vacuum in order to take high-resolution images of dried and coated foil samples. Dissected skin pieces were mechanically cleaned with a soft-tooth brush and placed into an ultrasonic cleaner for two minutes. Then, the skin was chemically cleaned by placing it in 6% sodium hypochlorite (NaOCl) for 30 s to remove any mucus. Both steps were repeated three times before a final cleaning in running water under pressure. Wet skin samples were dried under mild pressure for 24 h. All skin samples were extracted 0.5 cm downstream of the cut skin pieces for foil production (e.g. Figs 2, 3). For biomimetic materials, both the front surface and the underside plus a cross-section of a piece each from the riblet material and the Speedo® fabric were visualized in the ESEM. These samples were coated uniformly with platinum–palladium using a sputter coater (208 HR, Cressington Scientific Instruments, UK).

Although the skin pieces used for foil construction here were removed from the mid-body area to obtain single pieces that were large enough to be used for the foils, we also imaged denticle structure from various locations around the body. The basic structure of the denticles in the mid-body area with the three surface ridges (see Fig. 6) was similar to that seen in the tail and on the surfaces of the fins. Denticle morphology on the head was quite different from body denticle structure.

To estimate the wetted surface area of the shark skin foils, we measured the surface area of single denticles (e.g. Fig. 4) and used the number of denticles counted within an area of 1 mm^2 in the mako flat plate (Fig. 2) to provide an approximation of the total foil wetted surface area.

Foil manufacturing

For each of the foil materials described above, we took care to press the material onto the rigid foil surface by hand and to smooth out any wrinkles. No clamps were used, and strong pressure was not applied in order to prevent damage to the scales and membrane surface. The adhesive glues used (details provided above for each foil) worked well even after many flapping cycles in the water, and we did not observe separation of the two foil surfaces for any of the materials. Pieces of shark skin, removed and prepared as described above, were blotted dry and gently spread onto either the rigid foil or another piece of skin to which glue had been applied to the inner surface. Firm continuous pressure was all that was necessary to bond the two skin pieces together or to attach the skin to the rigid foil surface.

The different foil types used different pitch axes that depended on the material being studied. For the rigid foils (Fig. 2), the pitch axis was in the center of the foil. This allowed us to pitch the foil surface and, when combined with heave movement, produce a motion that was generally similar to that of the flexible foils. For the flexible foils (Fig. 3), the pitch axis was at the leading edge to hold the skin firmly and prevent any distortion of the flow by bending of skin in front of the pitch axis. All statistical comparisons of swimming speed were conducted among trials with a single foil design.

Flapping foil robotic apparatus

Movement of the rigid and flexible foils was controlled using a robotic flapping device, as described previously (Lauder et al., 2007; Lauder et al., 2011a; Lauder et al., 2011b). This robotic device (see Fig. 1) was mounted on a carriage attached to an air-bearing system to allow independent self-propulsion of an immersed foil with little frictional loss (see also Tangorra et al., 2011). A desired foil motion was specified using a custom LabVIEW program (LabVIEW 8, National Instruments, TX, USA). Under the condition of self-propulsion at a steady speed, the stroke-averaged thrust generated by the model must equal the average drag force experienced by the flapping foil (Lauder et al., 2007). During self-propulsion, we measured the flow-tank speed (U_{eq}) required for the foil to hold position at the equilibrium position (X_{eq}) and determined the SPS speed of different motion programs for changes in heave (amplitude in centimeters), pitch (maximal angle in degrees) and cycle speed (frequency in hertz). Amplitude values given here are ± the mean midline position. We determined an accurate U_{eq} using another custom LabVIEW program that tracked the x-position of the flapping foil by means of a magnetic linear encoder and the propeller speed by means of an optical rotary encoder to calculate an average U_{eq} for five slightly different flow speeds (for details, see Lauder et al., 2011a; Lauder et al., 2011b). Nine replicate trials were completed at each motion program setting for each foil.

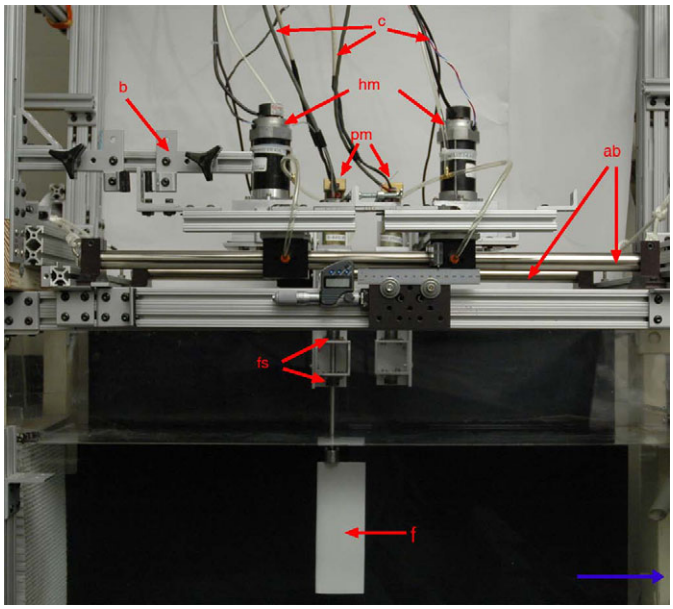

Fig. 1. The robotic flapping foil apparatus used to test the hydrodynamic function of shark skin and biomimetic models. Both rigid (f) and flexible foils with attached riblet material or shark skin are clamped in the flapper shaft (fs) and immersed in the flow tank. Robot motion is driven by a heave motor (hm) and a pitch motor (pm), mounted on air bearings (ab), so that the equilibrium position is only dependent on the cables (c). There is no cable effect as all tests are conducted at the equilibrium position (see Lauder et al., 2007; Lauder, 2011a; Lauder, 2001b) for details of this testing apparatus. Tuning the flume speed to match flapper thrust enables one to find the self-propelled speed (see text). Bumpers (b) limit large deflections. Note that the robot can drive two separate foils, but only one is used during the experiments here. The blue arrow indicates the flow direction. The rigid foil shown here is 19 cm in height, 6.85 cm in chord length (Fig. 2), but the membrane foils tested were a different shape (see text and Fig. 3 for a description).

Kinematics and hydrodynamic flow visualization

We took high-speed video sequences (using a FastCam 1024 PCI, Photron USA, CA, USA) during self-propelled speed experiments with the above-mentioned foils to document foil shape during swimming. Video data were acquired at 500 Hz, and each frame had a resolution of 1024×1024 pixels. Additionally, we trained 1.5-year-old spiny dogfish (*Squalus acanthias*; BL 27 cm) to swim steadily in the laboratory flow tank and recorded high-speed video sequences from a ventral view at swim speeds of 1.25 and 1.75 BL s^{-1}. Dogfish were obtained from local commercial vendors in Woods Hole, Massachusetts, USA. We determined *in vivo* body curvature from these live-shark videos and from the kinematic sequences of the mako membrane no. 2 foil by analysing three image frames from individual tail beats on which the shark body or the foil, respectively, showed the highest bending. Maximal body curvature was calculated from coordinates for three points within 2 cm distance along the edge of the curved body or foil, respectively. These data were used to ensure that our experiments using the flexible shark-skin foils were conducted using a motion program that replicated the *in vivo* curvatures of the lateral body surface of live freely swimming sharks.

Flow visualization was conducted for the mako flat plate and mako membrane no. 2 foils using DPIV, as described in our past research (Drucker and Lauder, 1999; Drucker and Lauder, 2002; Johansson and Lauder, 2004; Lauder et al., 2007). Briefly, water in

a 600 l recirculating flow tank was seeded with 6 g of hollow, silver-coated near-neutrally-buoyant glass particles. A 10 W continuous-wave argon-ion laser (Innova 300 Series, Coherent Laser Group, CA, USA) was focused onto a thin horizontal light sheet (1–2 mm thick) with a size of approximately 40×25 cm, which cut the foil at the midpoint on a plane halfway between top and bottom. Recorded images were analyzed with DPIV software (DaVis 7.2.2.272, LaVision, Göttingen, Germany).

Average Reynolds numbers (*Re*) and Strouhal numbers (*St*) for each self-propelling foil type are presented below in the Results section; in all cases, values for these dimensionless numbers are within the range of those found in studies of fish swimming *in vivo* (e.g. Flammang et al., 2011; Lauder and Tytell, 2006; Triantafyllou and Triantafyllou, 1995).

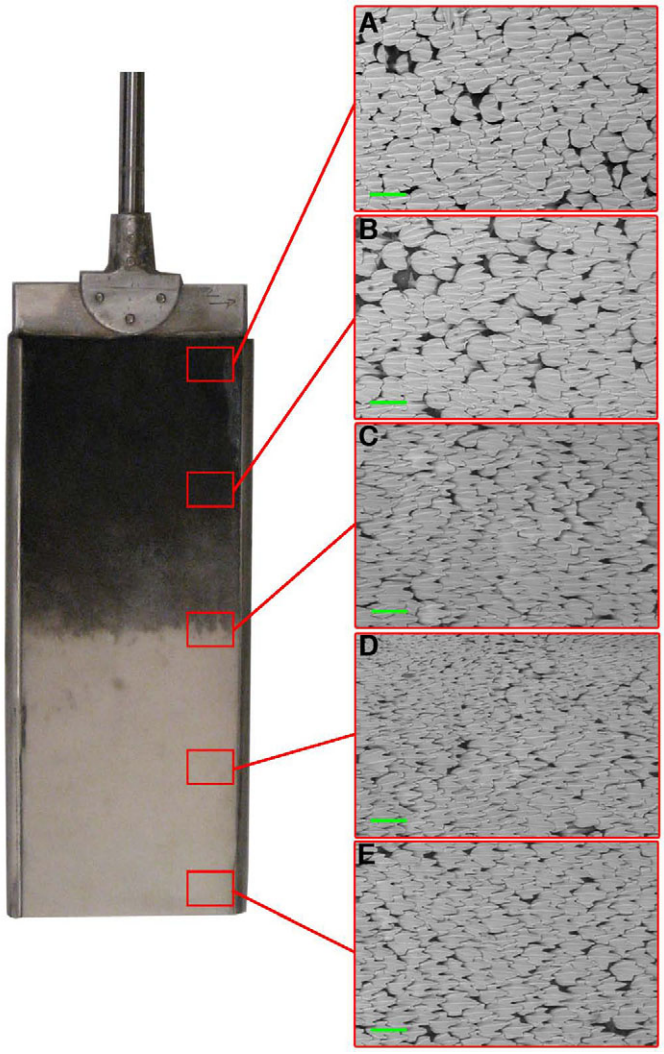

Fig. 2. Flat-plate foil (with rounded leading and trailing edges) covered with skin from the lateral midline area of a male shortfin mako shark (left). Dark skin color indicates skin from the lateral shark surface, whereas a whitish color indicates more ventral skin. The foil is 7.22 cm in chord length (width) and 19 cm in height (whereof 17.5 cm is covered with shark skin). Distribution of the skin structure on the surface of the mako flat-plate foil (right). Environmental scanning electron microscope (ESEM) images from parts of a top (A), a top middle (B), a middle (C), a middle bottom (D) and a bottom (E) area. Images were taken from skin pieces extracted 0.5 cm downstream of the right foil edge at each location. Scale bars, 200 μm. The leading edge of the denticles is on the left, and the natural water flow pattern would thus be left to right in this figure.

Statistics

Mean values and standard errors were calculated for the nine trials of the SPS speed measurements for each condition and are plotted in Figs 8–11, which show the results of the swimming speed trials. A Kolmogorov–Smirnov test verified the normal distribution of the nine trials in every case. Within each foil comparison set (e.g. shark skin with denticles facing out *versus* the sanded condition), we used an independent two-sample Student's *t*-test with equal sample sizes. Note that it is only appropriate to do corrected pairwise comparisons among each particular experimental treatment (such treatment conditions are plotted in the same color in Figs 8–11 to facilitate determination of which trials were compared statistically). Thus, we deliberately did not test for swimming speed differences among foils moved with different motion programs. Statistical tests were performed using SPSS 15.0 (SPSS, IL, USA).

RESULTS

Surface morphology

Images acquired by an ESEM of surface denticle structure and distribution for the mako flat plate are shown in Fig. 2, and for mako skin flexible membrane no. 2 are presented in Fig. 3. Denticle shape

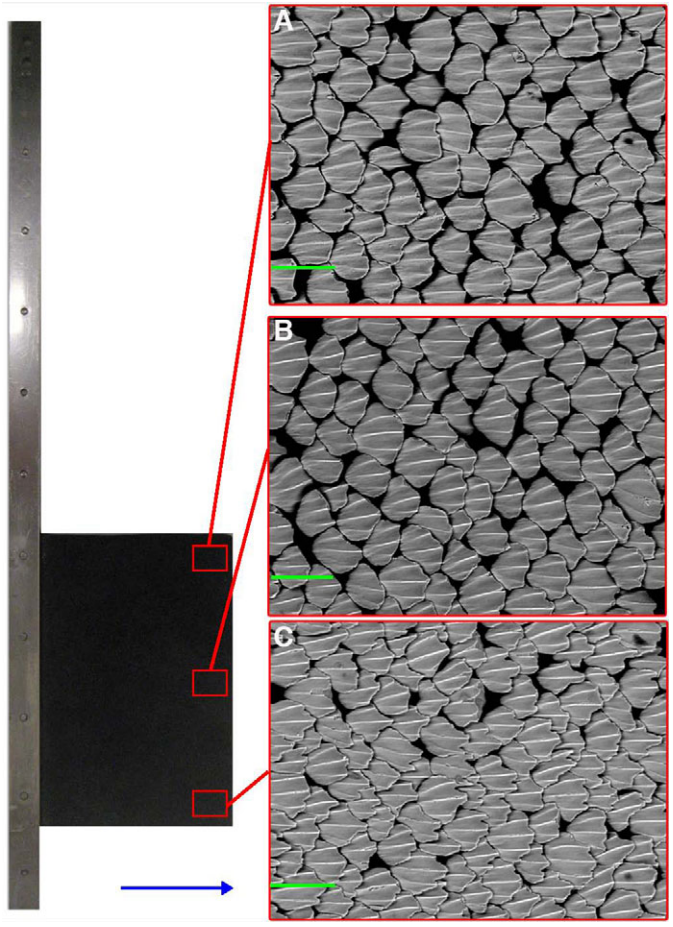

Fig. 3. Flexible shark skin foil mako membrane no. 1 (left). Bonded skin pieces (6.4 cm in length and 9.2 cm in height) of both lateral sides from 10 cm above the midline of a male shortfin mako shark are clamped 2.5 cm above the lower end in a sandwich bar holder. Right: distribution of skin structure on the surface of this mako membrane foil. ESEM images from parts of an upper (A), a middle (B) and a lower (C) area. Image samples were taken from skin pieces extracted 0.5 cm downstream of the foil edge of this foil at each location. The blue arrow indicates the direction of water flow during testing. Scale bars, 100 μm.

and size differ somewhat from top to the bottom of the foils. All denticles have three ridges with a spacing of 46–55 μm. Denticles on the mako flat plate range from 130 to 180 μm in width and from 180 to 210 μm in length. The denticles on the very top of the mako membrane no. 2 (Fig. 3A) have an oval shape, where the width (170–180 μm) is longer than the length (130–140 μm). Fig. 4 shows a highly magnified view of a single denticle, with three ridges and a toothed crown, from an area similar to that of Fig. 2D on the mako flat-plate foil.

Sanding the shark skin foils to reduce surface denticles to small nubs was successful, as seen in Fig. 5, where a part of the sanded mako membrane no. 1 foil is shown. The denticle surface was greatly reduced, and only small relics of the denticle bases and small remaining stubs seen in the upper left of Fig. 5 that escaped the sanding process remained. From ESEM images, we estimated that sanding the denticles (compare Figs 3 and 5) reduced the wetted surface area by >70%.

The underside (Fig. 6A) of the Speedo® 'shark skin' fabric shows a typical fabric surface with parallel seams. The seams on the surface of the outside 'biomimetic' surface (Fig. 6B) are slightly bigger and more significantly indented. Fig. 6C shows the cross-sectional morphology of two triangular dents in the outer surface that lie approximately 1.25 mm apart and form the biomimetic shark skin surface ornamentation. These indentations in the fabric are part of the biomimetic manufacturing process and vary slightly in size.

The outside of the riblet material (Fig. 7A) is covered with parallel tapering peaks (seen as white lines). The cross-section (Fig. 7B) provides a clearer view of the riblet structures, which have a scalloped shape, a height of 87 μm and a spacing of 340 μm. The underside of the material is smooth.

Self-propelled foil swimming speeds

The SPS trials for flexible membranes made of the Speedo® biomimetic fabric (Fig. 6; results shown in Fig. 8) showed that the 'shark skin' surface did not have a consistent effect of allowing increased swimming speeds for a given motion program. For example, moving the flexible Speedo® foil at 2 Hz with 2 cm heave when the ridges were in the vertical orientation did not result in any swimming speed change at all in comparison to a foil with the smoother inner fabric surface exposed to the water. When surface dents or ridges were oriented in a perpendicular orientation, swimming speeds of the foil slowed by an average of 5.2%. Adding a 20 deg pitch motion to the foil leading edge more than doubled the overall swimming speeds, but no clear effect of the biomimetic

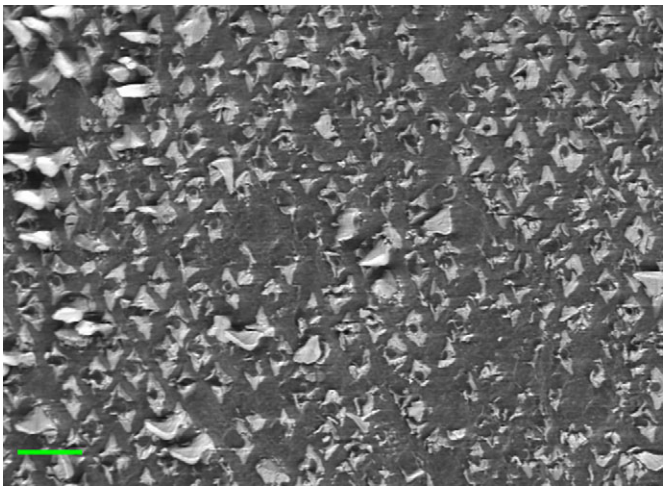

Fig. 5. An ESEM image of a part of the mako membrane no. 1 foil (Fig. 3) after the process of sanding. The full denticles are almost completely removed, with only small stubs remaining (compare with the intact denticle surface shown in Fig. 3). These stubs could not be removed without damaging the underlying collagen surface framework as denticles are embedded in the skin. Scale bar, 200 μm.

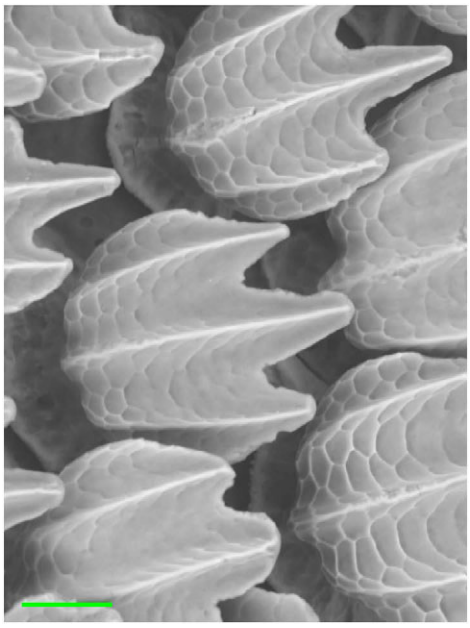

Fig. 4. Close-view ESEM image of denticles from the surface of the mid-body region in a bonnethead shark (*Sphyrna tiburo*) to show details of typical denticle structure with the three surface ridges and three posteriorly pointing prongs. Such denticle structure is common on the body, fins and tail, although denticles of this species on the head have a different morphology. Scale bar, 50 μm.

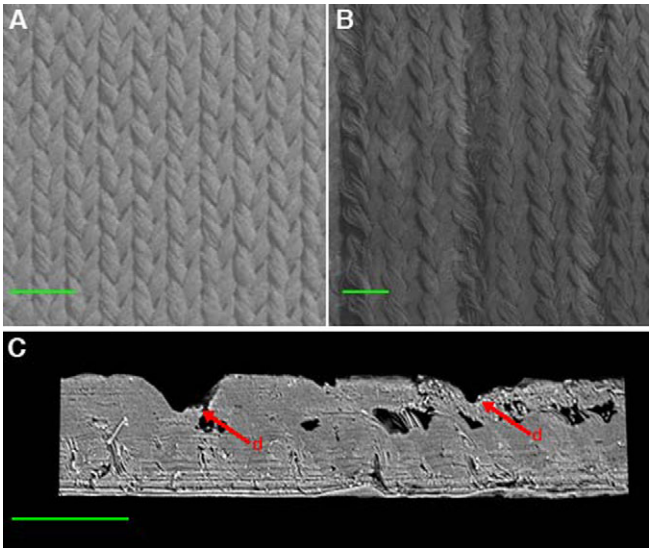

Fig. 6. ESEM images of Speedo® Fastskin FS II fabric. (A) Surface image of the underside (non-biomimetic) surface of the fabric. (B) Surface image of the outside (biomimetic surface) of the Speedo® fabric at the position of V-shaped printing. (C) Image of a cross-section of the Speedo® fabric, showing the dents on the biomimetic side (red arrows, 'd') in the fabric that generate the 'ribbed' surface. Scale bars, 500 μm.

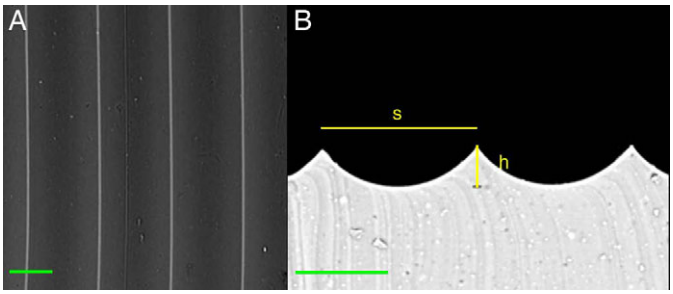

Fig. 7. ESEM images of the biomimetic riblet silicone material. (A) Front side of riblet surface with clearly visible height peaks (white lines). (B) Image of a cross-section showing the riblet structures with a height (h) of 87 μm and a spacing (s) of 340 μm. Scale bars, 200 μm.

surface could be detected (Fig. 8). Under 3 Hz actuation, the foil with the biomimetic surface on the outside actually swam slower than when the smoother inner fabric surface was exposed (Fig. 8). Speedo® biomimetic foils self-propelled at an average *Re* of 27,000 and an average *St* of 0.28 in these experiments.

Self-propelled swimming trials for rigid foils with a surface of the riblet material (Fig. 7; results shown in Fig. 9) showed a highly significant ($P<0.001$) increase in the SPS speed when the riblets were located on the outer surface of the foil compared with an inside orientation. The biggest difference was present at a motion program of 2 Hz, 1 cm heave and 0 deg pitch, where parallel-oriented riblets had a mean SPS speed of 35.6±0.3 cm s^{-1}, and the inside-oriented riblets a mean SPS speed of 32.5±0.4 cm s^{-1}, a 9.5% increase in self-propelled speed due to the riblet surface (values are means ± 1 s.e.m.). With the same motion program, the comparison of the parallel and perpendicular ridge orientations showed no significant difference. However, adding a pitch of 10 deg to the former motion program made the foil with perpendicular ridges propel significantly slower (2.5%) than the parallel foil, but both ridged foils self-propelled at a faster speed than the foils with a smooth surface. Riblet foils self-propelled at an average *Re* of 22,000 and an average *St* of 0.12 in these experiments.

Self-propelled speed trials for mako shark skin attached to the rigid flat plate (Fig. 2; results shown in Fig. 10) showed significant increases in swimming speed for all three motion programs when denticles were sanded off as compared with foils with intact denticles on the surface. Sanded foils swam at an average of 13.4% faster than foils with intact denticles in their normal orientation. When rigid mako skin foils were tested in the reverse orientation, only the 2 Hz, 1.5 cm heave, 10 deg pitch motion program showed a significant difference, and, in this case, the foil with the reverse orientation of denticles swam 11% faster (Fig. 10). Rigid mako shark skin foils self-propelled at an average *Re* of 24,000 and an average *St* of 0.22 in these experiments.

Self-propelled speed trials for mako and porbeagle skin made into a flexible membrane (Fig. 3; results shown in Fig. 11) showed that, for all eight test conditions, sanding the denticles reduced the swimming speed by an average of 12.3%. Seven of the eight comparisons were significantly different, and only the 2 Hz, 2 cm heave and 30 deg pitch motion program failed to be significantly different. The most striking difference was obtained with the mako membrane no. 1 at a motion program of 2 Hz, 2 cm and 0 deg pitch (see Fig. 11A), for which the intact foil (mean SPS: 19.7±0.15 cm s^{-1}) swam almost 20% faster than the sanded foil (mean SPS: 16.3±0.13 cm s^{-1}). Flexible shark skin foils self-propelled at an average *Re* of 13,000 and an average *St* of 0.37 in these experiments.

We emphasize that this is the opposite result to that obtained with the rigid foils described above: for flexible shark skin membranes, removing the denticles slows down swimming speed; if shark skin is attached to a rigid foil, sanding the denticles can increase swimming speed.

Kinematics and hydrodynamics

Freely swimming spiny dogfish displayed mean body curvatures of 0.14±0.01 cm^{-1} (mean ± 1 s.e.m.) swimming at 1.25 BL s^{-1} (*Re*=90,000) and 0.20±0.01 cm^{-1} at 1.75 BL s^{-1} (*Re*=127,000). For comparison, we measured the curvatures of flexible mako membrane no. 2, which showed mean curvature values of 0.17±0.01, 0.18±0.01 and 0.25±0.01 cm^{-1} for the three different motion programs at the relevant self-propelled speeds. The swimming flexible shark skin membranes studied here thus achieved curvature values comparable to those of freely swimming live sharks at commonly observed cruising speeds.

In order to understand better the mechanism of thrust generation by flexible shark skin foils, and the hydrodynamic basis of the performance difference between the normal and sanded flexible shark skin membranes, we quantified fluid flow over the flexible and rigid foil surface during self-propulsion by using DPIV. Sample analyses are shown in Figs 12 and 13.

The flexible shark skin membrane foils, moved with a motion program of 2 Hz, ±2 cm heave and 10 deg pitch, showed a clear leading-edge vortex (LEV) that remained attached to the foil for most of the flapping cycle (Fig. 12). This LEV moved posteriorly down the foil from its initial position near the leading edge (see

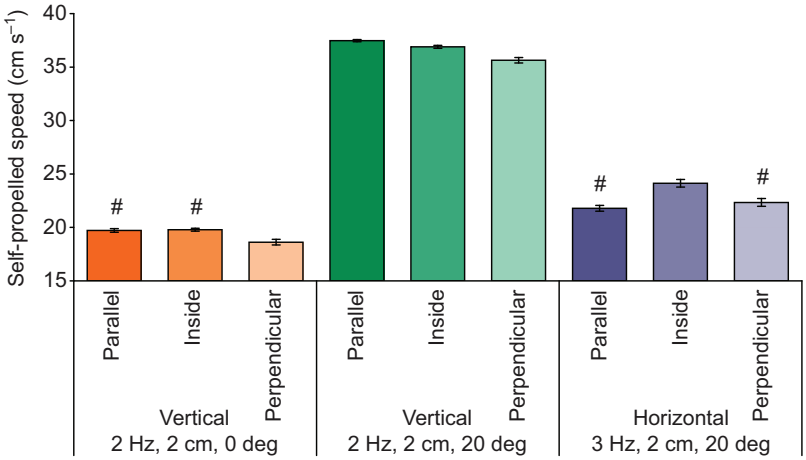

Fig. 8. Histogram of the mean self-propelled speed results (mean from *N*=9 trials for each test) for Speedo® membrane foils. Error bars are ±1 s.e.m. The motion program settings below each group of similarly colored bars show the programmed foil movement, defined by frequency (Hz), amplitude (cm) and pitch (deg). Speedo® fabric was tested on two different foil orientations (vertical and horizontal – see Materials and methods) and with the biomimetic surface ridges parallel to the free-stream flow, perpendicular to the free-stream flow and 'inside' or reverse orientation, with the biomimetic surface on the inside glued to the foil and the non-biomimetic surface exposed to the water. Within each group of similarly colored bars, bars with # symbols are not significantly different from each other ($P>0.05$). All other comparisons have a level of significance between $P<0.05$ and $P>0.0001$.

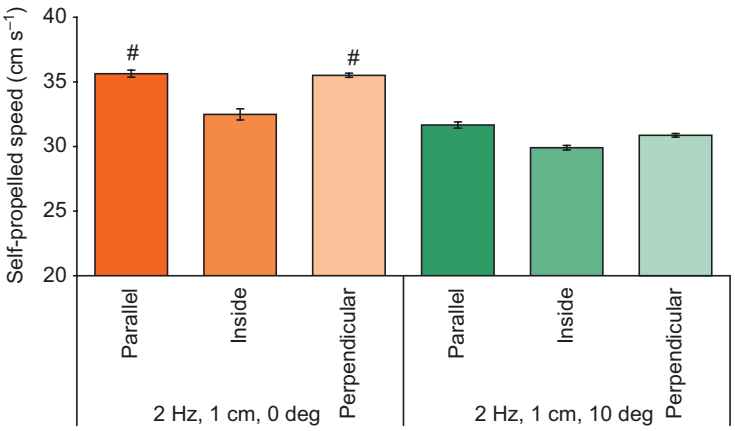

Fig. 9. Histogram of the mean self-propelled speed (mean from nine trials for each test) for the silicone riblet material applied to a NACA 0012 foil surface. Error bars are ±1 s.e.m. The motion program settings below each group of similarly colored bars show the programmed foil movement, defined by frequency (Hz), amplitude (cm) and pitch (deg). Silicone riblet material was tested with the biomimetic surface ridges parallel to the free-stream flow, perpendicular to free-stream flow and 'inside' or reverse orientation, with the riblet surface on the inside glued to the foil and the non-biomimetic (smooth) surface exposed to the water. Within each group of similarly colored bars, bars with # symbols are not significantly different from each other (P>0.05). All other comparisons have a level of significance between P<0.05 and P>0.000. On average, the foils with the 'inside' orientation propel at a 7.2% slower self-propelled swimming (SPS) speed than the foils with parallel-oriented ridges.

Fig. 12, 300–400 ms time-frames) and was then shed into the wake before reforming at the leading edge as the flapping cycle resumed. Plots of flow velocity in the x-direction (parallel to free-stream flow, V_x) *versus* the distance from the foil surface are shown for six frames (0, 100, 200, 300, 400, 500 ms) representing 100% of a motion cycle in Fig. 12. The attached LEV is clearly seen by the negative velocities (portions of the curve to the left of the zero line in Fig. 12) that occur near the foil surface where flow is reversed relative to free-stream velocities (e.g. Fig. 12, 100 ms time-point). Along the transect away from the foil surface, flow velocities change sign as the LEV core is traversed, and, at a distance of approximately 3 cm from the foil surface, the free-stream velocity has been reached.

Comparisons of the flow pattern at the foil leading edge between shark skin foils with denticles on the surface and those with the denticles sanded off show substantial differences in LEV location for the flexible membrane shark skin foils, but not for the flat-plate foils, corresponding well to the differences in self-propelled speed reported above for flat-plate *versus* membrane shark skin foils (Figs 10, 11). Fig. 13A shows the analysis of LEV vorticity for the intact and sanded mako flat-plate foil at a motion program of 2 Hz, 2 cm and 10 deg. This plot shows that the peak vorticity, which reflects the vortex core location, appears at almost the same distance from the foil edge in the two rigid foils. The intact foil has a peak vorticity of 13.6 s^{-1} at a distance of 11.3 mm from the foil edge, whereas the sanded foil peak vorticity of 11.4 s^{-1} occurs at a distance of 11.9 mm from the sanded foil edge.

The analogous plot for the intact and the sanded flexible mako membrane no. 2 foil at a motion program of 2 Hz, 2 cm and 10 deg is shown in Fig. 13B. Here, the intact foil shows a peak vorticity of 9.5 s^{-1}, which occurs at a distance of 6.3 mm from the foil surface. In contrast, the sanded foil has a maximal vorticity of 11.1 s^{-1} at a distance of 14.5 mm from the foil surface. Sanding the denticles on the flexible foil membrane leads to a displacement of the LEV core a distance of nearly a centimeter (8.2 mm) further away from the foil surface.

DISCUSSION

In this paper, we have compared the swimming performance of both rigid and flexible shark skin foils under both intact and sanded conditions, with the aim of quantifying the possible locomotor benefits of the surface denticles on the skin. In addition, we analyzed the swimming performance of two biomimetic shark skin surfaces, a ribbed rubber material and the Speedo® Fastskin fabric, which possesses surface indentations.

Our most noteworthy results were: (1) that the shark denticles had no beneficial locomotor effect on the moving rigid shark skin foils, and in fact the unmodified rigid foils swam more slowly than those on which the denticles had been removed for two motion programs (Fig. 10), (2) that surface denticles did improve swimming performance significantly (by an average of 12.3%) on flexible shark skin membrane foils compared with those in which the denticles had been removed and (3) that biomimetic surface indentations and riblets can enhance swimming performance under certain motion programs, but not for other types of foil movement.

These data emphasize both the utility of using a highly controlled robotic system to test for changes in swimming performance, and the importance of flexibility in locomotor dynamics: studying flexible shark skin membranes proved essential to demonstrating a significant increase in locomotor performance due to surface

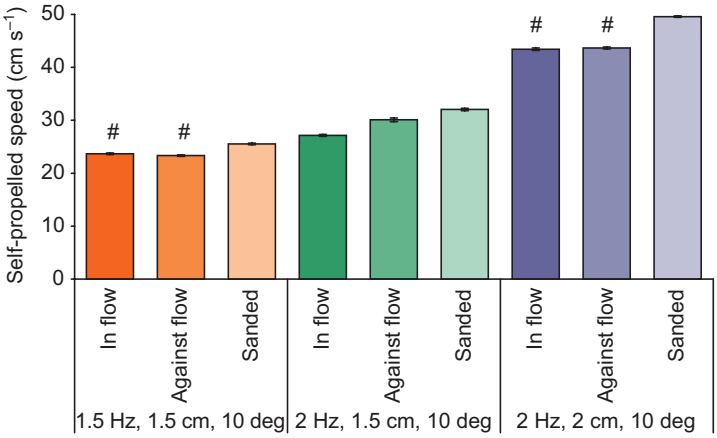

Fig. 10. Histogram of the mean self-propelled speed results (mean from nine trials for each test) for the mako shark skin attached to a rigid flat plate. Error bars are ±1 s.e.m. The motion program settings below each group of similarly colored bars show the programmed foil movement, defined by frequency (Hz), amplitude (cm) and pitch (deg). Mako shark skin on the flat plate was tested with the denticle surface oriented parallel to the free-stream flow in the same direction as on a living shark ('in flow'), oriented opposite to the *in vivo* shark denticle orientation ('against flow') and sanded, where most of the denticle surface had been removed (Fig. 5). Within each group of similarly colored bars, bars with # symbols are not significantly different from each other (P>0.05). All other comparisons have a level of significance between P<0.05 and P>0.0001. On average, the sanded rigid foils propel at a speed 13.4% higher than that of the foils with denticles, with a maximum difference of 18.03% (P<0.001) at a motion program of 2 Hz, 1.5 cm and 10 deg.

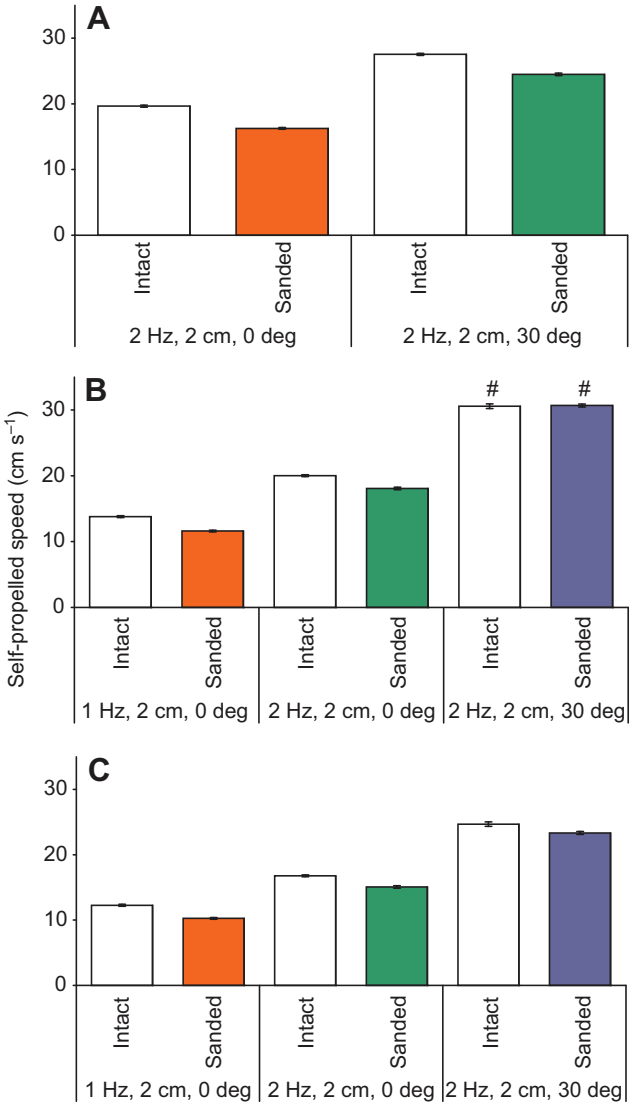

Fig. 11. Histogram of the mean self-propelled speed results (mean from nine trials for each bar) for the flexible moving shark skin membranes. (A) mako membrane no. 1, (B) mako membrane no. 2 and (C) porbeagle membrane. Error bars are ±1 s.e.m. The motion program settings below each group of similarly colored bars show the programmed foil movement, defined by frequency (Hz), amplitude (cm) and pitch (deg). Shark skin membranes were tested intact, with denticles oriented as in live sharks, and sanded, where most of the denticle surface had been removed (Fig. 5). All paired comparisons within similar motion programs had a level of significance between $P<0.001$ and $P>0.0001$. The sanded foils swim at an average speed 12.3% lower than that of the intact foils.

ornamentation. In addition, as we discuss below, shark skin denticles might enhance thrust in addition to causing a reduction in drag.

Flapping foils and shark swimming

How closely did swimming by our flexible shark skin membranes match the locomotor conditions evident in live sharks? The shark skin foils in this study self-propelled at average Strouhal numbers between 0.28 and 0.38, which is well within the range of the Strouhal numbers used by live sharks. Many fishes, including sharks, swim at Strouhal numbers between 0.21 and 0.41 (Flammang et al., 2011; Lauder and Tytell, 2006; Triantafyllou and Triantafyllou, 1995). The Reynolds numbers during flexible shark skin foil self-propulsion were also in the range of swimming by smaller sharks that typically cruise at swimming speeds of 0.5 to 1.0 BL s^{-1} – 13,000 to 24,000 – although certainly large open-water sharks swim at much higher Reynolds numbers during fast swimming or during periods of burst accelerations. As our foils were self-propelling, they swam at their natural Strouhal and Reynolds numbers under the driven motion program, and we could not alter these parameters experimentally without removing the self-propelled condition.

Surface curvatures achieved by the flexible shark skin foils could also have a potentially important influence on locomotor performance as surface denticles might be expected to bristle as the skin is bent and thus alter flow near the skin (e.g. Lang et al., 2008). We compared the measured surface curvatures of our flexible shark skin foils with those we measured in live sharks swimming in our laboratory flow tank, and the values of 0.17–0.25 cm^{-1} for foils accord well with measured maximal mid-body values from live spiny dogfish swimming at 1.0 BL s^{-1} (0.14–0.20 cm^{-1}). Body curvature values vary considerably in swimming sharks, depending on location and swimming speed, from 0 to 0.3 cm^{-1}, so these curvature measurements show that the shark skin membranes when self-propelling bend to an extent to similar to that of the skin of a live shark during unrestrained locomotion.

Swimming of biomimetic foils

Self-propelled speed results from the Speedo® material foils under conditions with the biomimetic surface oriented towards the water *versus* located inside away from the water show that swimming performance depends on the motion program used and the orientation of the surface ridges (Fig. 8). For two of the three motion programs used, the biomimetic surface actually reduced swimming performance compared with flexible Speedo® foils with the underside located towards the water surface. The orientation of surface ridges can also have a significant effect on swimming performance, and placing the surface ridges in an orientation perpendicular to the oncoming flow reduced swimming performance for all three motion programs.

The proposed drag-reduction properties of Speedo® Fastskin surface ridges is thus called into question when the locomotion of this material made into flexible foils is compared with that of controls with no surface indentations. While it is theoretically possible that both skin friction reduction and pressure drag reduction could be increased by the surface of this material (Benjanuvatra et al., 2002), the complexities of surface deformation in human swimmers and the three-dimensional flows that occur over the body during movement suggest that there is no consistent flow direction over the surface ornamentation on body suits made of this material. Our ESEM images (Fig. 6) of the Speedo® fabric also evoke doubts about whether the swimsuit surface functions as shark-skin-like riblets as the surface indentations bear little resemblance to either shark skin or engineered riblet materials (e.g. Fig. 7). Manufactured riblet materials have sharp longitudinal rib structures (Bechert and Bartenwerfer, 1989) that can cause alterations in boundary layer flow (Fig. 7). A cross-cut of the Speedo® material shows dents instead of ribs, with large distances between the dents. If we treat these dents as riblets, the height to spacing (h:s) ratio would be ~0.1. A two-dimensional riblet surface with h:s=0.1 resulted in a maximal passive drag reduction of 0.5% (Bechert et al., 2000), supporting our results of either no drag reduction or drag enhancement with impaired swimming performance resulting from the Speedo® material.

Our studies of self-propelled speeds achieved with the engineered riblet material (Fig. 7) show that improvements in swimming speed through drag reduction can occur depending on the way in which

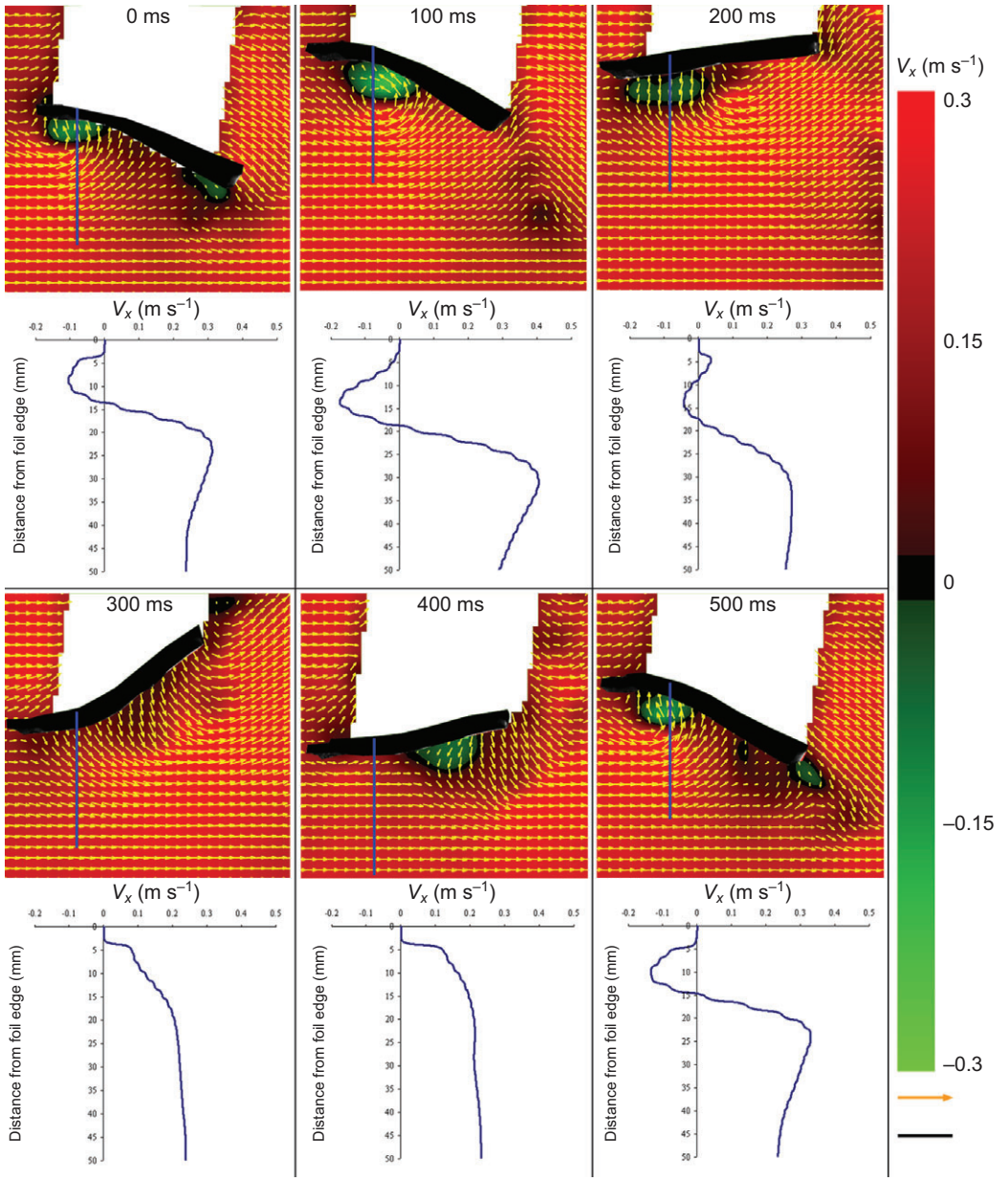

Fig. 12. Time series of flow velocities over a whole motion cycle of the normal mako shark skin membrane no. 2 foil, swimming at its average self-propelled speed of 0.2 m s^{-1} (motion program: 2 Hz, 2 cm heave, 0 deg pitch). For the cycle period of 500 ms, images (above) and plots (below) of 0, 100, 200, 300, 400 and 500 ms are shown. A cycle begins and ends at 0 ms and 500 ms, respectively. Yellow arrows in DPIV images show velocity vectors. Colored contours indicate the velocity in the *x*-direction (V_x) of a downstream (red) and upstream (green) moving fluid. The foil shape at each time is overlaid on each image. Black scale bar, 2 cm. The orange scale vector represents 1 m s^{-1} and indicates the flow direction from left to right. Values for V_x are taken along the blue lines and plotted against the distance from the foil edge in the V_x-plots. The blue line starts 3–4 mm above the lower foil edge. In this area, V_x values approximate zero, and so the actual foil edge begins at the point where the V_x-plots shows the first slope. Note that negative velocities, where the flow travels upstream, occur near the foil edge. White areas above the foil membrane indicate areas that were in shadow, and so no vectors were calculated in these regions.

the material is moved (Fig. 9). We also altered the orientation of the riblets and compared parallel and perpendicular orientations. Placing the riblet surface on the inside so that the foil had a smooth outer surface *reduced* swimming performance, suggesting that the riblets were effective in reducing drag: when riblets were exposed to the flow in a parallel orientation, they improved swimming speeds by up to 9.5%. But both parallel and perpendicular orientations improved swimming performance, suggesting that the surface roughness was more important than the precise orientation of the riblets.

Our ESEM images revealed a h:s ratio of 0.25 for this riblet material (Fig. 7). Bechert and colleagues (Bechert et al., 2000) studied a system with adjustable longitudinal slit riblets that yielded a motionless drag reduction (riblet foils were held still in moving flow) of approximately 5% at a h:s ratio of 0.2. Our data confirm previous studies that riblets can reduce not only the motionless drag (Bechert and Bartenwerfer, 1989; Bechert et al., 1997; Luchini and Trombetta, 1995) but also the drag in-motion, when foils with riblet surfaces self-propel.

Swimming of shark-skin foils

One mechanism of reducing drag during locomotion is to reduce skin friction drag, and the magnitude of skin friction drag force depends on the wetted surface area (Hoerner, 1965). We estimate that sanding the denticles reduced the wetted surface area of the flexible foils by 70%. If this were the only factor in understanding shark skin locomotor function, then the sanded foils would be exposed to a skin friction drag force that is much less than the force acting on the intact foils, and sanded foils would self-propel at higher speeds than the foils with denticles intact.

However, flexible shark skin foils actually showed a substantial improvement in swimming performance of an average of 12.3% (with a maximal improvement of almost 20%) as compared with the same foils with the surface denticles sanded off. Orienting the denticle crown tips against the flow stream, opposite to the natural alignment, still did not reduce swimming performance to the degree produced by sanding the foil surface (Fig. 10) but did reduce swimming performance compared with the natural orientation for the 2 Hz, 1.5 cm heave, 0 deg pitch motion program.

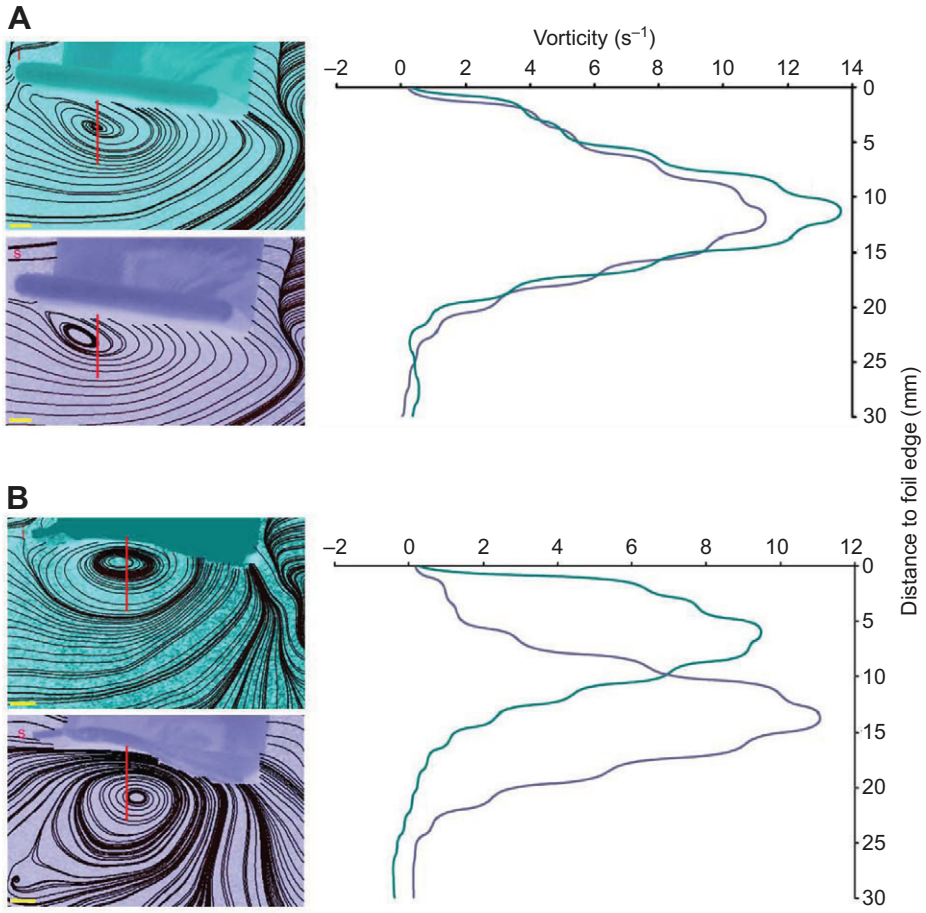

Fig. 13. Images of streamlines showing flow patterns of an identical position in the motion cycle of the intact (i, cyan, upper panel) and the sanded (s, pale purple, lower panel) from a mako shark skin attached to the rigid flat plate (A) with a motion program of 2 Hz, 2 cm heave and 10 deg pitch and the mako membrane no. 2 flexible foil (B) with a motion program of 2 Hz, 2 cm heave and 30 deg pitch. Values for the vorticity near the intact (i) and the sanded (s) foils are taken along the red line transects and plotted against the distance from the foil edge on the right. Note that the position of maximal vorticity is much farther away from the flexible foil surface on the sanded foil than for the intact foil with denticles. Yellow scale bars, 1 cm; flow direction is from left to right.

Interestingly, the same treatments applied to a rigid foil did not have the same effect: sanding the surface of shark skin applied to a rigid foil increased the self-propelled speed – an effect opposite to that seen in flexible foils. These results show the substantial effect that flexibility of the swimming surface can have on the results of foil surface tests and indicate that future testing of shark skin drag-reduction effects should include flexible surfaces that are freely swimming and approximate the bending seen *in vivo* by swimming sharks – other conditions might not show a drag-reduction effect.

Hydrodynamic function of shark skin

We were able to detect significant differences in the pattern of water flow over the swimming shark skin flexible foils for normal *versus* sanded surfaces (Figs 12, 13), and these hydrodynamic differences can help explain why flexible foils with the sanded surface swam more slowly compared with those with the intact surface denticles. DPIV showed the presence of a LEV on the swimming foils that is located at a greater distance from the foil surface after sanding the denticles than in the intact foil with normal denticles (Fig. 13B). The presence of denticles on the surface thus alters the flow environment near the flexing foil surface in such a manner that the LEV adheres more closely to the foil surface than it does after the denticles are sanded off.

Vortices are regions of low pressure with a pressure minimum at the vortex core (Rossi, 2000). The low-pressure zone of the leading-edge core will affect suction forces on the foil surface, and this pressure force acts normal to a surface in fluids (Sigloch, 2005). This pressure vector can be divided into two resultant forces (normal to each other), one acting along the free-stream direction, whereas the other acts orthogonal to this path. Appropriate foil orientations where the inclined surface with an attached LEV is angled upstream (Fig. 12, 0–100 ms) will result in enhanced propulsion through leading-edge suction as one component of the low-pressure vector will draw the foil upstream. At these positive angles of attack, the force parallel to the flow points upstream, and so it represents a thrust force. The lower the pressure on the foil surface and the closer the vortex core is to the foil surface, the higher the thrust force. We predict that the LEV-derived suction (thrust) force is reduced after sanding the denticles, which alters flow near the membrane surface and causes the LEV to move almost 1 cm further away from the leading-edge surface of the moving foil. This would reduce leading-edge suction and hence thrust.

This result suggests that one important effect of the skin denticles is to enhance thrust, and not simply to reduce drag. The overwhelming emphasis of the existing literature on shark skin has been on drag reduction, but denticles alter vortex location, and, especially on the tail surface where flow separation and vortex formation have been demonstrated (Wilga and Lauder, 2002; Wilga and Lauder, 2004), could increase thrust. Similar effects of denticles could occur on pectoral fins also, where vortices are generated during maneuvering (Wilga and Lauder, 2000), and denticles that enhance vortex attachment to the fin surface would increase lift and hence maneuvering forces.

The precise nature of flow modification on the foil surface when denticles are present is not known at present, and studying this will require close views (on the order of 1–2 mm^2 field of view) of the flows on the surface of moving shark skin foils. This is certainly a challenging proposition *in vivo*, but will likely reveal the specifics of flow modification due to surface denticles on the skin as

compared with a sanded condition. Indeed, the question of what flow modification occurs in the boundary layer region in the presence of natural shark skin denticles during self-propulsion remains unanswered at present and remains a key area for future study.

ACKNOWLEDGEMENTS

We thank Vern Baker and Erik Anderson for assistance with the flapper programming and experiments and all members of the Lauder lab and the MCZ Fish Department (Karsten Hartel and Andy Williston) for their assistance with this project. Special thanks to Brooke Flammang for videos of spiny dogfish.

FUNDING

This work was supported by National Science Foundation grants IBN0316675 and EFRI-0938043 to G.V.L.

REFERENCES

Anderson, E. J., McGillis, W. and Grosenbaugh, M. A. (2001). The boundary layer of swimming fish. *J. Exp. Biol.* **204**, 81-102.

Applegate, S. (1967). A survey of shark hard parts. In *Sharks, Skates and Rays* (ed. W. C. Hamlett) pp. 37-67. Baltimore, MD: Johns Hopkins University Press.

Bechert, D. and Bartenwerfer, M. (1989). The viscous flow on surfaces with longitudinal ribs. *J. Fluid Mech.* **206**, 105-129.

Bechert, D. W., Hoppe, G. and Reif, W. E. (1985). On the drag reduction of the shark skin. In *AIAA Shear Flow Control Conference*, vol. AIAA 85-0546, pp. 1-18. Boulder, CO: AIAA.

Bechert, D. W., Bruse, M., Hage, W., van der Hoeven, J. and Hoppe, G. (1997). Experiments on drag-reducing surfaces and their optimization with an adjustable geometry. *J. Fluid Mech.* **338**, 59-87.

Bechert, D. W., Bruse, M. and Hage, W. (2000). Experiments with three-dimensional riblets as an idealized model of shark skin. *Exp. Fluids* **28**, 403-412.

Benjanuvatra, N., Dawson, G. and Blanksby, B. (2002). Comparison of buoyancy, passive and net active drag forces between Fastskin TM and standard swimsuits. *J. Sci. Med. Sport* **5**, 115-123.

Büttner, C. C. and Schulz, U. (2011). Shark skin inspired riblet structures as aerodynamically optimized high temperature coatings for blades of aeroengines. *Smart Mater. Struct.* **20**, 094016.

Castro, J. I. (2011). *The Sharks of North America.* Oxford: Oxford University Press.

Dinkelacker, A., Nitschke-Kowsky, P. and Reif, W. (1987). On the possibility of drag reduction with the help of longitudinal ridges in the walls. In *Proceedings of the IUTAM Symposium on Turbulence Management and Relaminarization*, pp. 109–120. Bangalore, India: Springer Verlag.

Drucker, E. G. and Lauder, G. V. (1999). Locomotor forces on a swimming fish: three-dimensional vortex wake dynamics quantified using digital particle image velocimetry. *J. Exp. Biol.* **202**, 2393-2412.

Drucker, E. G. and Lauder, G. V. (2002). Experimental hydrodynamics of fish locomotion: functional insights from wake visualization. *Integr. Comp. Biol.* **42**, 243-257.

Flammang, B. E., Lauder, G. V., Troolin, D. R. and Strand, T. (2011). Volumetric imaging of shark tail hydrodynamics reveals a three-dimensional dual-ring vortex wake structure. *Proc. R. Soc. B* **278**, 3670-3678.

Han, X., Zhang, D., Li, X. and Li, Y. (2008). Bio-replicated forming of the biomimetic drag-reducing surfaces in large area based on shark skin. *Chinese Sci. Bull.* **53**, 1587-1592.

Hoerner, S. F. (1965). *Fluid-dynamic Drag*: *Practical Information on Aerodynamic Drag and Hydrodynamic Resistance.* Midland Park, NJ.

Johansson, L. C. and Lauder, G. V. (2004). Hydrodynamics of surface swimming in leopard frogs (*Rana pipiens*). *J. Exp. Biol.* **207**, 3945-3958.

Koeltzsch, K., Dinkelacker, A. and Grundmann, R. (2002). Flow over convergent and divergent wall riblets. *Exp. Fluids* **33**, 346-350.

Lang, A. W., Motta, P., Hidalgo, P. and Westcott, M. (2008). Bristled shark skin: a microgeometry for boundary layer control? *Bioinsp. Biomimet.* **3**, 046005.

Lauder, G. V. and Tytell, E. D. (2006). Hydrodynamics of undulatory propulsion. In *Fish Biomechanics*, Vol. 23 (ed. R. E. Shadwick and G. V. Lauder), pp. 425-468. San Diego, CA: Academic Press.

Lauder, G. V., Anderson, E. J., Tangorra, J. and Madden, P. G. (2007). Fish biorobotics: kinematics and hydrodynamics of self-propulsion. *J. Exp. Biol.* **210**, 2767-2780.

Lauder, G., Madden, P. G. A., Tangorra, J., Anderson, E. and Baker, T. V. (2011a). Bioinspiration from fish for smart material design and function. *Smart Mater. Struct.* **20,** doi:10.1088/0964-1726/20/9/094014.

Lauder, G., Tangorra, J., Lim, J., Shelton, R., Witt, C. and Anderson, E. J. (2011b). Robotic models for studying undulatory locomotion in fishes. *Marine Tech. Soc. J.* **45,** 41-55.

Luchini, P. and Trombetta, G. (1995). Effects of riblets upon flow stability. *Flow Turb. Combust.* **54**, 313-321.

Luchini, P., Manzo, F. and Pozzi, A. (1991). Resistance of a grooved surface to parallel flow and cross-flow. *J. Fluid Mech.* **228**, 87-109.

Mollendorf, J., Termin, A., Openheim, E. and Pendergast, D. (2004). Effect of swim suit design on passive drag. *Med. Sci. Sports Exer.* **36**, 1029-1035.

Neumann, D. and Dinkelacker, A. (1991). Drag measurements on V-grooved surfaces on a body of revolution in axial flow. *Appl. Sci. Res.* **48**, 105-114.

Reif, W. E. (1982). Morphogenesis and function of the squamation in sharks. 1. Comparative functional morphology of shark scales, and ecology of scales. *Neues Jah. Geol. Palaeon. Abh.* **164**, 172-183.

Reif, W. E. (1985). *Squamation and ecology of sharks.* Stuttgart: Senckenbergische Naturforschende Gesellschaft.

Rossi, M. (2000). Of vortices and vortical layers: an overview. In *Vortex Structure and Dynamics* (ed. A. Maurel and P. Petitjeans), pp. 40-123. Berlin: Springer.

Schultz, W. W. and Webb, P. W. (2002). Power requirements for swimming: do new methods resolve old questions? *Integr. Comp. Biol.* **42**, 1018-1025.

Sigloch, H. (2005). *Technische Fluidmechanik.* Berlin: Springer.

Tangorra, J., Phelan, C., Esposito, C. and Lauder, G. (2011). Use of biorobotic models of highly deformable fins for studying the mechanics and control of fin forces in fishes. *Integr. Comp. Biol.* **51,** 176-189.

Toussaint, H., Truijens, M., Elzinga, M., Van De Ven, A., De Best, H., Snabel, B. and De Groot, G. (2002). Effect of a Fastskin bodysuit on drag during front crawl swimming. *Int. Soc. Biomech. Sports* **1**, 1-10.

Triantafyllou, M. S. and Triantafyllou, G. S. (1995). An efficient swimming machine. *Sci. Amer.* **272**, 64-70.

Tytell, E. D. (2007). Do trout swim better than eels? Challenges for estimating performance based on the wake of self-propelled bodies. *Exp. Fluids* **43**, 701-712.

Tytell, E. D., Borazjani, I., Sotiropoulos, F., Baker, T. V., Anderson, E. J. and Lauder, G. V. (2010). Disentangling the functional roles of morphology and motion in the swimming of fish. *Integr. Comp. Biol.* **50**, 1140-1154.

Wilga, C. D. and Lauder, G. V. (2000). Three-dimensional kinematics and wake structure of the pectoral fins during locomotion in leopard sharks *Triakis semifasciata*. *J. Exp. Biol.* **203**, 2261-2278.

Wilga, C. D. and Lauder, G. V. (2002). Function of the heterocercal tail in sharks: quantitative wake dynamics during steady horizontal swimming and vertical maneuvering. *J. Exp. Biol.* **205**, 2365-2374.

Wilga, C. D. and Lauder, G. V. (2004). Hydrodynamic function of the shark's tail. *Nature* **430**, 850.